

Effect of Transport Layer on Polymer - Fullerene Derivative Bulk Heterojunction Organic Photovoltaic Cell Performance using Transmission Circuit Model Analysis

K. L. Usha Kumary^{1*}, M. Pratheek², A. Ashfak³, T. A. Shahul Hameed⁴ and P. Predeep²

¹LBS Centre for Science and Technology, Trivandrum, Kerala, 695033, India.

²Laboratory for Molecular Electronics and Photonics, National Institute of Technology, Calicut, Kerala, 673601, India.

³Department of Mechanical Engineering, TKM College of Engineering, Kollam, Kerala, 691005, India.

⁴Department of Electronics and Communication Engineering, TKM College of Engineering, Kollam, Kerala, 691005, India.

Received 14 September 2020, Revised 21 December 2020, Accepted 8 May 2021

ABSTRACT

Polymer-fullerene derivative bulk heterojunction (BHJ) organic photovoltaic cell (OPV) is one of the encouraging devices to harvest solar energy where transport layers carry the momentous role in performance and stability. In this work, the effect of C₆₀ as an electron transport layer in a BHJ device composed of Poly(3-hexylthiophene-2,5-diyl) (P3HT) and [6,6]-Phenyl-C₆₁-butyric acid methyl ester (PCBM) is investigated by impedance spectroscopy (IS) and modelled using circuit models – the transmission circuit (TC) model and electrochemical polarization model. The effective lifetime and mobility of carriers were also extracted. It is seen that the fullerene C₆₀ transport layer effectively reduces bulk resistance with biasing voltage.

Keywords: Carrier Transport, Impedance and Mobility

1. INTRODUCTION

The organic photovoltaic (OPV) cells are known for the unique properties of lightweight, lower manufacturing cost, flexibility and ease of processing. Introducing new materials as donors or acceptors, modifying the properties of the existing materials through varying processing conditions or modifying the device architecture contribute to enhance the performance, though bulk heterojunction formed by intermixing donor and acceptor materials is more popular due to many aspects. When light hits the active layer, excitons are generated and diffused towards the donor/acceptor interface. The excitons at the interface are separated into charge carriers and collected by the respective electrodes. During these processes, normally if the active layer thickness exceeds 200nm, light absorption reaches about 90% [1] and in the bulk heterojunction, efficient dissociation takes place due to high charge separation at the interfaces. The remaining processes of carrier transport and collection by the electrodes carry a remarkable role in the efficiency of OPVs. Because of the efficient dissociation and high mobility of carriers, P3HT:PCBM BHJ is preferred in most OPVs [2].

In the conventional or inverted device, the nature of electrical contact at the donor and acceptor with the respective electrodes is very critical to the performance. Ideal ohmic contact at the active layer/electrodes interface with less barrier height is better for effective carrier transport,

* Corresponding Author: ushakumarykl@gmail.com

extraction at the electrodes and reduced carrier recombination and it leads to the study of new materials with better interfacial properties reducing the barrier height that minimizes the carrier recombination and enhancement of short circuit current density. The materials also act as optical spacers to concentrate the incident light to the active layer [3].

Fullerene and its derivatives, known for their application as acceptors, are also used as electron transport materials that block the opposite carriers. C_{60} is a small molecule organic semiconductor and its thin layer can be prepared by vacuum deposition method which has the advantage of purifying the material through sublimation which favours the device lifetime and the performance. It has been reported that the device performance is improved with 20nm C_{60} as an electron transport layer (ETL) compared to the ultra-thin layer [4]. In the OPV, the cathode work function affects the device performance just like that of the anode work function and it must match the lowest unoccupied molecular orbital (LUMO) of the electron acceptor for better performance. The electron transport layer provides an ohmic contact with the acceptor material, transports negative carriers, and in turn improves the efficiency of the cathode [5]. The carrier concentration, lifetime and mobility under varying biasing voltages and intensities [6] can be determined using impedance spectroscopy (IS).

In this paper, C_{60} with a thickness of 20nm is used as the transport layer to minimize the barrier height at the cathode in a bulk heterojunction OPV device. Its impact is analysed using impedance spectroscopy which helps to study the physical processes that take place in the sample. The device is also modelled using a transmission circuit and electrochemical polarization models by which the recombination resistance and chemical capacitance were determined.

2. MATERIAL AND METHODS

The OPV device was constructed with the composition ITO/MoO₃/P3HT:PCBM/ C_{60} /Al and the materials chemical structure [7][8], energy level diagram [4][9] and layout of the device are given in Figure 1. The materials P3HT, PCBM and C_{60} from Sigma-Aldrich were used for constructing the device. As part of the substrate cleaning, ITO coated glass substrates (76Ω/cm²) were sonicated in Hellmanex solution (0.1%) and isopropyl alcohol and subjected to ozone treatment. The composite of P3HT and PCBM was formed with a weight ratio of 1:1 in 1,2-dichlorobenzene and kept at a temperature of 70°C with stirring for 12hrs [10][11]. The hole transport layer (HTL), MoO₃ was coated upon the ITO substrate and above it, a blend of P3HT and PCBM was layered by spin coating at 1000rpm for a duration of 65s and annealed at 130°C for 15min in a Ika C-MAG HS7 hotplate. Vacuum evaporation at 10⁻⁵ torr with thickness monitoring was used to coat C_{60} as ETL and Al cathode. Electrical characterizations of the device were made by Keithley Source Meter along with a Solar Simulator at 100mW/cm². Impedance spectroscopy was implemented to obtain information regarding the carrier dynamics inside the device which governs its performance. The Precision Impedance Analyser (Wayne Kerr 6500B) was used to plot the response of the device when an ac voltage of 50mV/10mV applied with different bias voltages.

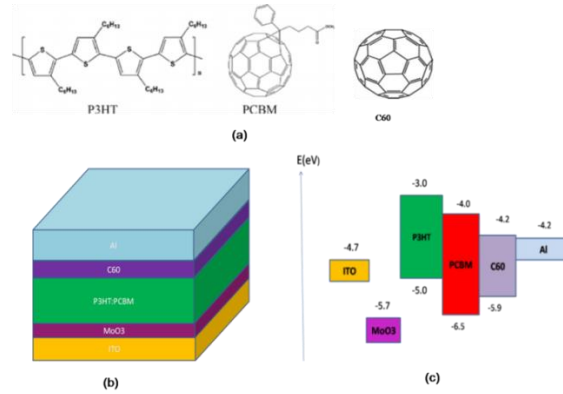


Figure 1. Structures of (a) P3HT, PCBM and C₆₀ (b) OPV device and (c) energy level diagram

3. RESULTS AND DISCUSSION

The device characteristics under dark and light are given in Figure 2. The various parameters V_{oc} (open circuit voltage), J_{sc} (short circuit current density), PCE (power conversion efficiency) and fill factor with C₆₀ of 20nm thickness as ETL are presented in Table 1.

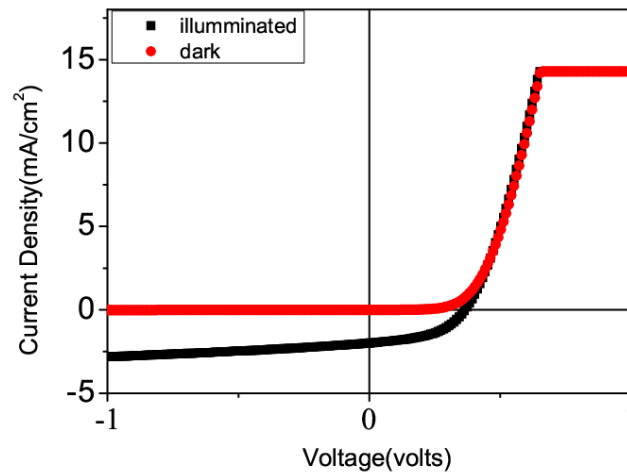


Figure 2. J-V characteristics

Table 1. Photovoltaic parameters of the device measured under the illumination of 100mW/cm²

V_{oc} (volt)	J_{sc} (mA/cm ²)	Fill Factor (%)	PCE (%)	R_s (Ω)	R_{sh} (Ω)
0.368	1.99	46.9	0.34	46.17	735.29

The lower value of V_{oc} indicates a poor ohmic contact and the low series resistance R_s favours a higher fill factor [12][13]. The introduction of transport layers mainly affects the photovoltaic parameter V_{oc} which can attain its maximum in case of an ohmic contact and its effect reflects in the fill factor and PCE. The higher forward current (dark) in Figure 2 signifies a better electron extraction [5].

The variations of capacitance, resistance and conductance are plotted for different dc voltages from -1V to 0.4V. Capacitance is measured with an ac signal of amplitudes 10mV and 50mV and its variation as shown in Figure 3 is found to be more significant when the biasing voltage is made more positive. For a constant bias voltage, capacitance reduces at mid-frequency due to the injected carriers and it continuously increases at lower frequencies due to the extra capacitance present. It implies that the deep defect states are present at frequencies below 1kHz and from 1kHz to 10kHz, the capacitance monotonically decreases with an increase in active layer thickness [14]. At high frequency, the capacitance attains a steady value due to the absence of ac charges which matches with the computed device capacitance using the expression $C = \epsilon A/d$ [15].

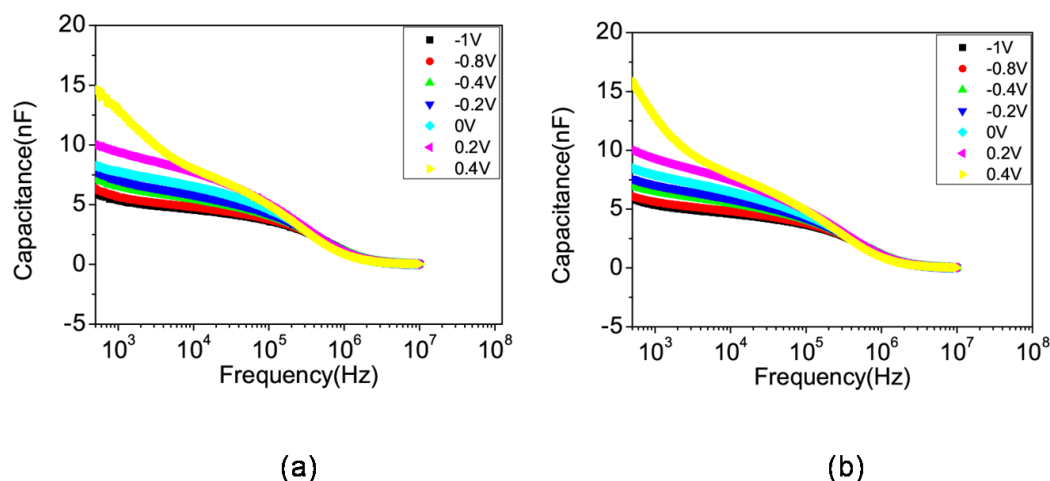


Figure 3. Capacitance variation with amplitudes (a) 10mV and (b) 50mV and biasing voltages

As the reverse bias increases, the increase in the width of the depletion region spreads into the entire active layer thickness which causes a reduction in the capacitance and thus the capacitance transition disappears. Finally, the junction capacitance C_d becomes closer to that of geometric capacitance C_g . In Figure 3, for all biasing voltages, the capacitance value $>10^6$ Hz is C_g while the junction capacitance C_d can be obtained up to 10^4 Hz and the transition between those frequencies is not due to the defects [14]. The measured conductance and resistance are plotted in Figure 4. It is obvious that as the bias voltage increases, conductance increases and reaches a steady increase when the bias voltage becomes more positive due to the injected carriers.

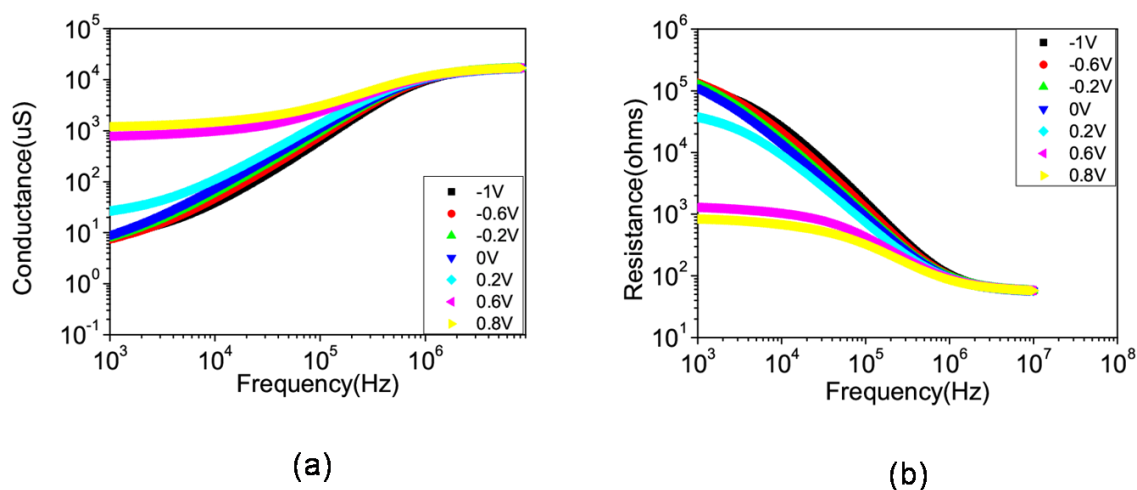


Figure 4. (a) Conductance and (b) resistance variation with frequency

The impedance (both real and imaginary) variation with frequency for various biasing voltages is shown in Figure 5. The impedance in the low frequency region (<100Hz) shown in Figure 5(a) corresponds to R_s+R_p and at high frequency (>100kHz), it is only R_s which is not affected by the biasing voltage. The value of R_s+R_p reduces with the increase in biasing voltage and the smaller value of R_p signifies better carrier transport. The relaxation frequency (f_p) can be determined from Figure 5(b) and it is centred at the peak which is shifted to higher frequencies as the biasing voltage increases. The characteristic relaxation time $\tau=1/\omega_p$ reduces with the increase in the biasing voltage and the small value of τ indicates that the dissociation of excitons takes place efficiently at the BHJ and also the transport of carriers contributes to the parameters J_{sc} and V_{oc} [16][17].

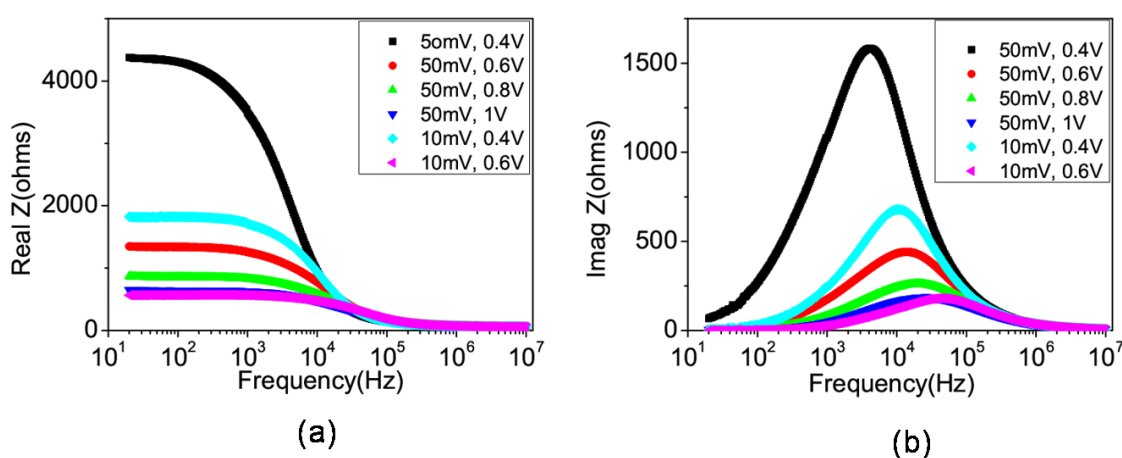


Figure 5. Impedance (a) real part and (b) imaginary part vs frequency

The TC model provides quantitative information about the processes taking place in the device and it is used to analyse the diffusion and recombination of carriers in the photoactive layer. In the model shown in Figure 6, R_{tr} represents the process of diffusion at high frequencies (transport resistance) and R_r corresponds to the recombination of carriers at low frequencies (recombination resistance). The capacitance related to the excess of charge carrier storage is called the chemical capacitance C_c and C_g is the geometric capacitance. The series resistance R_s is the resistance due to the substrate and contacts of the OPV device.

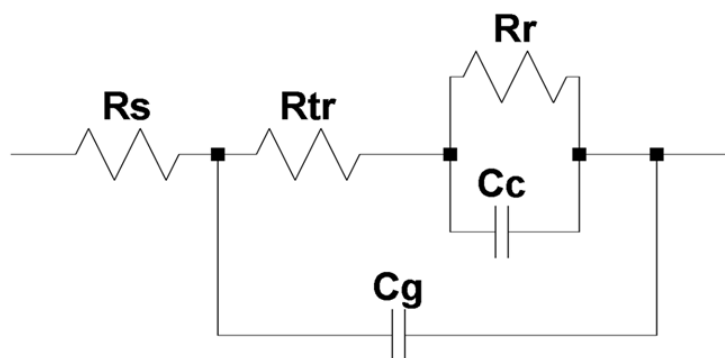


Figure 6. TC model

Based on the coupled diffusion and recombination processes, carrier transport is determined [18]. The time constants that correspond to the diffusion and recombination processes are $\tau_d = R_{tr}C_c$ and $\tau_{rec} = R_rC_c$ respectively. The elements R and C in $R_{tr}C_c$ consists of bulk resistance and capacitance which includes both geometric and the one due to illumination. The $R_{tr}C_c$ represents the high frequency region and R_rC_c corresponds to the low frequency region. The impedance response with different biasing voltages at frequencies varied over the range from 20Hz to 10MHz is obtained as in Figure 7. A 10mV/50mV signal is used to perturb the system. It is to be noted that the semicircle diameter reduces with increase in the biasing voltage which is attributed to the transport of charge carriers at the transport layer/active layer interface [19].

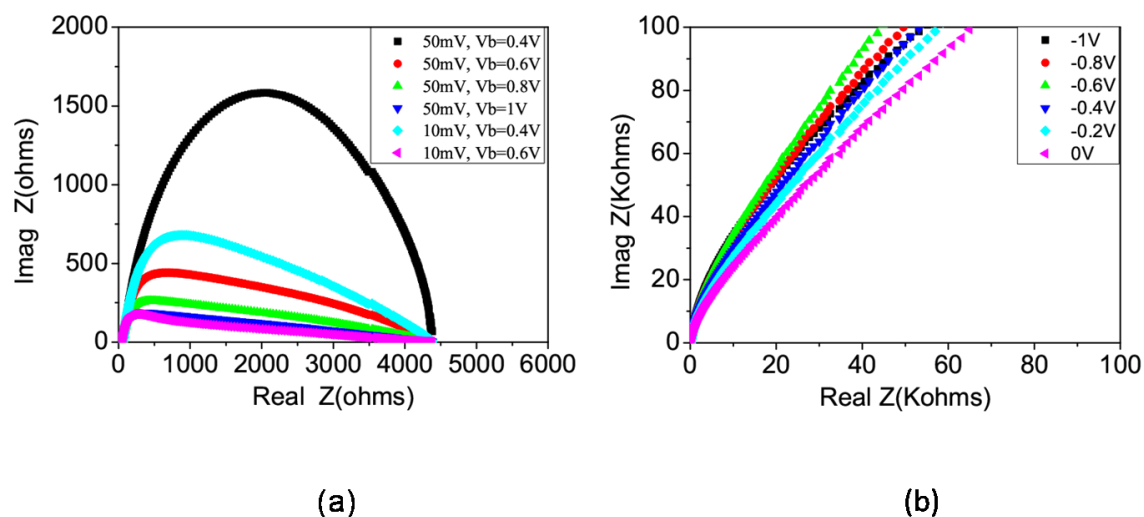


Figure 7. Nyquist plot with (a) positive biasing voltages and (b) negative biasing voltages

It is assumed that there is a balance in the charge injection and transport and no carrier concentration gradient exists in the device. Hence, recombination is less, i.e., $\tau_d < \tau_{rec}$ [18] which implies $R_{tr} \ll R_r$ and thus, the TC model can be simplified to the electrochemical polarisation model as given in Figure 8. It consists of the resistance R_s in series with a resistor R_p in parallel with a capacitance C_p . The resistance R_s represents the resistance due to the substrate and contacts of the device. The resistance R_p and C_p are the circuit elements that represent the transport effects.

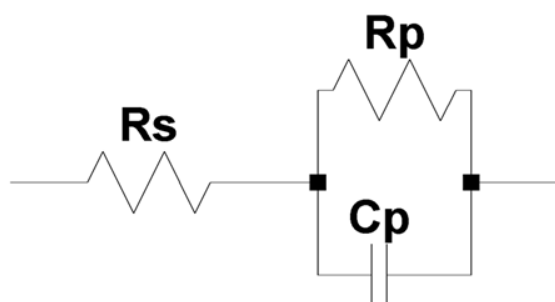
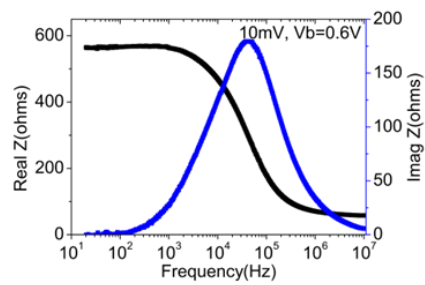
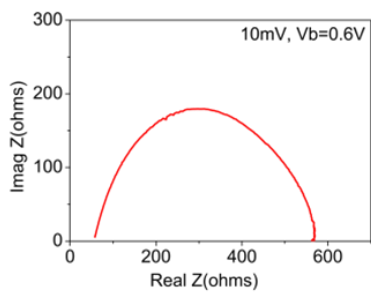
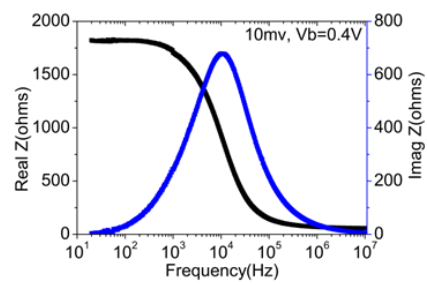
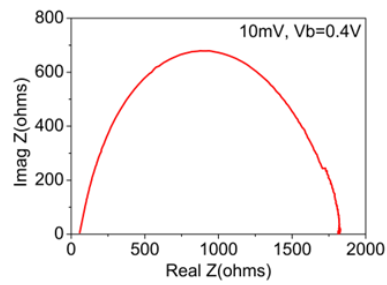
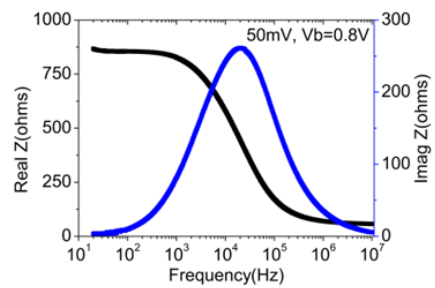
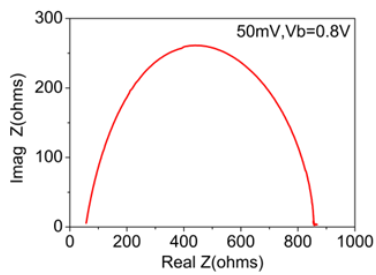
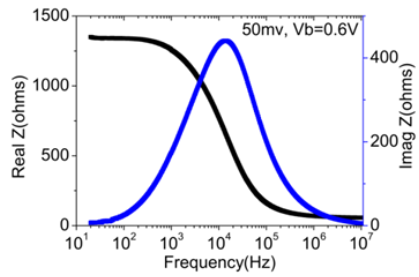
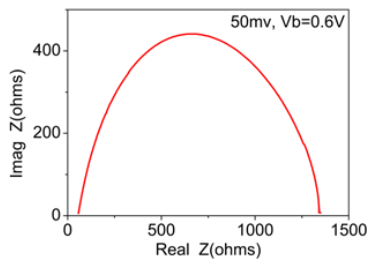
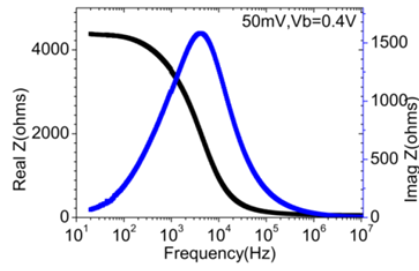
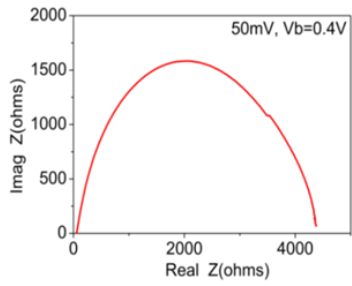


Figure 8. Equivalent circuit model

The morphology of the structure and the interface modification by the transport layers could reduce the contact resistance in OPVs. The responses with different biasing voltages are separately shown in Figure 9 and also the parameters obtained are given in Table 2.



(a)

(b)

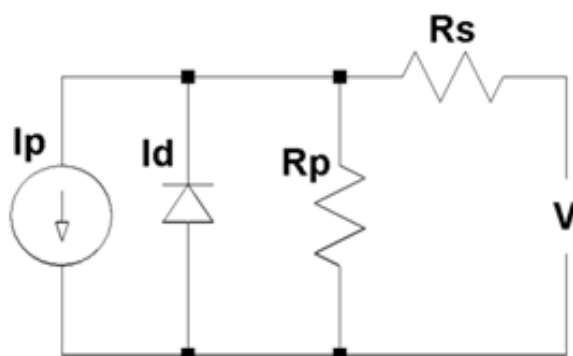
Figure 9. (a) Nyquist plot and (b) Bode plot**Table 2.** Parameters obtained for an R-RC circuit

AC Signal Amplitude (mV)	Biasing Voltage V _b (V)	R _s (Ω)	R _p (Ω)	C _p (nF)	τ (μS)
50	0.4	57.98	4323.17	9.24	39.95
50	0.6	57.16	1287.41	9.10	11.72
50	0.8	57.16	800.23	9.60	7.68
50	1.0	57.16	584.84	10.14	5.93
10	0.4	58.07	1758.40	9.04	15.89
10	0.6	58.07	510.50	8.09	4.13

From Table 2, it is understood that the value of R_s does not vary with the applied bias for a fixed signal amplitude [6] and a proportional slight change is seen in its value with a change in the amplitude, whereas R_p reduces with the increase in biasing voltage. The small value of shunt resistance R_p represents more efficient charge transport [16]. With the addition of C₆₀ as ETL, a reduction is observed in the values of R_p and the lifetime [13]. The I-V characteristic of photovoltaic cell [18][20] is given by

$$I = I_p - I_o \left\{ \exp \left[\frac{V + IR_s}{nV_t} \right] - 1 \right\} - \frac{V + IR_s}{R_p} \quad (1)$$

where I_o is the dark current, n - ideality factor, $V_t = \frac{kT}{q}$, the thermal voltage, k - Boltzmann constant, T - absolute temperature, q - electron charge and I_p represents the light-generated current. The diode equivalent circuit is given in Figure 10.

**Figure 10.** Diode model equivalent

Carrier mobility was obtained from the negative differential susceptance plot shown in Figure 11. The relaxation peak occurs at τ_r^{-1} and the average transit time τ_{dc} is obtained as $0.8306\mu\text{s}$ from the expression $\tau_{dc} = 0.56\tau_r$ [18].

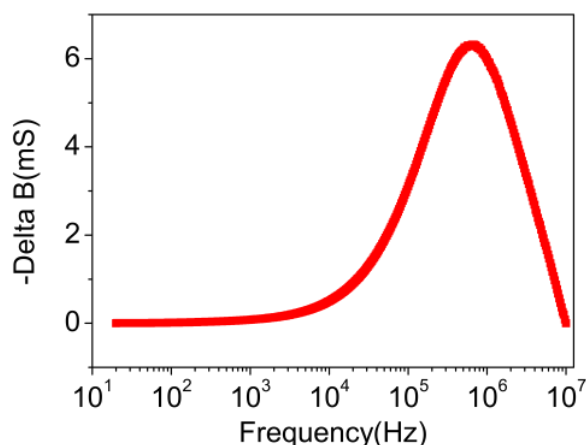


Figure 11. Negative differential susceptance plot

With the τ_{dc} , the carrier mobility is computed as $3.00 \times 10^{-4} \text{ cm}^2/\text{Vs}$. PCE increases with the increase in mobility due to the faster movement of carriers towards the electrodes under the built-in electric field. The mobility value lies in the range 10^{-3} to $10^{-4} \text{ cm}^2/\text{Vs}$ provides a better PCE for a P3HT:PCBM bulk heterojunction OPV [21].

4. CONCLUSION

A polymer - fullerene derivative bulk heterojunction organic photovoltaic device with C_{60} as ETL was fabricated and the J-V characteristics were obtained under the dark and the light conditions. Electrical characteristics were studied using impedance spectroscopy in the dark with 10mV/50mV ac signal and superimposing with bias voltages. The negative differential susceptance method is used to compute the carrier mobility and it is obtained as $3.00 \times 10^{-4} \text{ cm}^2/\text{Vs}$. The Nyquist and Bode plots were obtained. The device is simulated and studied using a transmission model and finally reduced to the electrochemical (R-RC) model. It is observed that bulk resistance and lifetime reduce with the increase in biasing voltage which is attributed to the charge transfer at the transport/active layer interface. Compared to the device without ETL, the carrier lifetime in the present device reduces more than 50% and also demonstrated that the transmission circuit model is an effective method to study the working of organic photovoltaic cells.

ACKNOWLEDGEMENTS

The corresponding author acknowledges the financial support provided from TEQIP-II, Phase-II, TKMCE/TQP/019/18 dated 27/02/2018, a World Bank Project at TKM College of Engineering, Kollam-5, Kerala, India. The acknowledgements are also due for the laboratory facilities used in LAMP, Department of Physics, National Institute of Technology, Calicut, Kerala, India and the support rendered by Sree Ayyappa College, Chengannur, Kerala, India.

REFERENCES

- [1] Yu, H., Li, Y., Dong, Y., Huang, X., Int. J. Photoenergy **2016**, (2016) 1–9.

- [2] Erray, M., Hanine, M., Boufounas, E., El Amrani, A., *Eur. Phys. J. Appl. Phys.* **82**, (2018) 30201-30214.
- [3] Hou, W., Xiao, Y., Han, G., Lin, J-Y., *Polymers* **11**, 1 (2019) 143-185.
- [4] Golubev, T., Liu, D., Lunt, R., Duxbury, P., *AIP Advances* **9**, 3 (2019) 035026-035031.
- [5] Martinez, M. M. F., Neculqueo, G., Bernede, J. C., Cattin, L., *Phys. Status Solidi A* **212**, 8 (2015) 1767-1773.
- [6] Oklobia, O., Komilian, S., Sadat-Shafai, T., *Org. Electron.* **61**, (2018) 276–281.
- [7] Huang, W., Gann, E., Cheng, Y-B., McNeill, C. R., *ACS Appl. Mater. Interfaces* **7**, 25 (2015) 14026-14034.
- [8] Irwin, M. D., Buchholtz, D. B., Hains, A. W., Chang, R. P. H., Marks, T. J., *PNAS* **105**, 8 (2008) 2783-2787.
- [9] Barr, M. C., Carbonera, C., Po, R., Bulović, V., Gleason, K. K., *Appl. Phys. Lett.* **100**, 18 (2012) 183301-183304.
- [10] K. L. Usha Kumary, M. Pratheek, T. A. Shahul Hameed, P. Predeep, "Measurement of hole mobility in P3HT based photovoltaic cell using space charge limited current method," *AIP Conference Proceedings*, (2019) 020142-020146.
- [11] K. L. Usha Kumary, M. Pratheek, T. A. Shahul Hameed, P. Predeep, "Admittance spectroscopy in the measurement of hole mobility in organic photovoltaic cell," *AIP Conference Proceedings*, (2020) 020016-020021.
- [12] El Jouad, Z., Barkat, L., Stephant, N., Cattin, L., Hamzaoui, N., Khelil, A., Ghamnia, M., Addou, M., Morsli, M., Bechu, S., Cabanetos, C., Richard-Plouet, M., Blanchard, P., Bernede, J. C., *J. Phys. Chem. Solids* **98**, (2016) 128-135.
- [13] El Jouad, Z., Cattin, L., Martinez, F., Neculqueo, G., Louarn, G., Addou, M., Predeep, P., Jayan Manuel, Bernede, J. C., *Eur. Phys. J. Appl. Phys.* **74**, 2 (2016) 24603-24608.
- [14] Xu, L., Wang, J., Hsu, J. W. P., *Phys. Rev. Appl.* **6**, 6 (2016) 064020-064029.
- [15] von Hauff, E., *J. Phys. Chem. C* **123**, 18 (2019) 11329-11346.
- [16] Ghann, W., Sobhi, H., Kang, H., Chavez-gil, T., Nesbitt, F., Uddin, J., *J. Chem. Eng. Mater. Sci.* **5**, (2017) 46-66.
- [17] Kobori, T., Kamata, N., Fukuda, T., *Adv. Mater. Phys. Chem.* **07**, 08 (2017) 323–333.
- [18] Li, Z., Guo, W., Liu, C., Zhang, X., Li, S., Guo, J., Zhang, L., *Phys. Chem. Chem. Phys.* **19**, 31 (2017) 20839-20846.
- [19] Li, X., Xie, F., Zhang, S., Hou, J., Choy, W. C. H., *Light: Science & Applications* **4**, (2015) 1–7.
- [20] Rathore, N., Panwar, N. L., Yettou, F., Gama, *Int. J. Ambient Energy* (2019) 1-18.
- [21] Hacene, S. B., Benouaz, T., *Phys. Status Solidi A* **21**, 4 (2014) 862-868.